Detailed simulations of the effect of particle deformation and particle-fluid heat transfer on particle-particle interactions in liquids

Available online at www.sciencedirect.com

ScienceDirect

Procedia Engineering 102 (2015) 1563 – 1572

Procedia Engineering

www.elsevier.com/locate/procedia

The 7th World Congress on Particle Technology (WCPT7)

Detailed simulations of the effect of particle deformation and particle-fluid heat transfer on particle-particle interactions in liquids

Henrik Ström*, Srdjan Sasic

Division of Fluid Dynamics, Department of Applied Mechanics, Chalmers University of Technology, SE-412 96 Göteborg, Sweden

Abstract

A multiphase DNS (direct numerical simulation) method is used to investigate two types of particle-particle interactions relevant in dispersed liquid-solid flows: the interaction between two solid particles under non-isothermal conditions, and the interaction between a solid particle and a deforming particle (e.g. a bubble). It is shown that the drafting, kissing and tumbling sequence of two sedimenting solid particles can be significantly affected by the presence of simultaneous particle-fluid heat transfer. For small but finite internal particle heat sources, the drafting sequence is faster and the interaction is speeded up. However, for larger internal heat sources, the kissing and tumbling events may be inhibited altogether by the natural convection currents developing around the particles. In addition, isothermal interactions between a solid particle and a bubble are investigated. It is shown that the particle-bubble attachment process may be significantly altered under conditions of lowered surface tension (i.e. after addition of surfactants) due to an increased tendency for the bubble to deform.

Selection and peer-review under responsibility of Chinese Society of Particuology, Institute of Process Engineering, Chinese Academy of Sciences (CAS)

Keywords: Liquid-solid flow; Particulate flow; Heat transfer; Bubble-particle interaction; Computational fluid dynamics

1. Introduction

Many important industrial processes involve dispersed solid or deformable (i.e. droplets and bubbles) particles suspended in a liquid carrier phase. Upon interacting, dispersed entities may come together to form a new "phase" – often called aggregates. Such systems represent a particularly challenging form of multiphase flows, but are of high

* Corresponding author. Tel.: +46-31-772-13-60; fax: +46-31-18-09-76.
E-mail address: henrik.strom@chalmers.se

Selection and peer-review under responsibility of Chinese Society of Particuology, Institute of Process Engineering, Chinese Academy of Sciences (CAS)
doi:10.1016/j.proeng.2015.01.292

industrial significance. Important examples include flotation equipment (for treatment of waste-water [1], recycled paper [2] or minerals [3,4]) and a range of operations within the petrochemical industry [5,6].

In flotation processes for water treatment, for example, solid particles and bubbles interact to form buoyant agglomerates that rise to the surface. The efficiency, robustness and adaptability of a flotation process are therefore highly dependent on the thermal and hydrodynamic interactions between the various phases. Another example where such interactions are of utmost importance is in heterogeneous catalytic processes involving liquid-solid flow, where suspended catalyst particles move in a carrier fluid of similar density whilst heat is released in the catalyzed chemical reactions.

In order to facilitate the derivation of useful macroscopic models for the interactions among several particles in an averaged description of the flow, direct numerical simulations (DNS) at the microlevel are indispensable. With such DNS techniques, the Navier-Stokes equations are solved directly, together with a method for taking the presence of particles into account. Some of the most common multiphase DNS methods include the Volume of Fluid (VOF) method [7], the front tracking method [8], the immersed boundary methods [9-13], and Lagrange multiplier/fictitious domain methods [14-18]. In addition, there exist methods where the fluid flow near an immersed object is locally matched to the corresponding Stokes flow solution [19]. Although DNS of multiphase systems with simultaneous heat transfer and solid particles motion is still an emerging field, a number of methods have already been presented in the literature, based on the distributed Lagrange multiplier/fictitious domain method [20, 21], the immersed-boundary method [22] or by accomplishing the fluid-solid coupling at the level of the discrete momentum and thermal energy balance equations [23].

For applications also involving fluid-like particles, the VOF multiphase model is considered an appropriate framework [24]. Furthermore, among multiphase DNS techniques, the VOF model is relatively simple to implement and computationally efficient since it avoids explicit computation of the hydrodynamic force and torque on the particles [25]. In the current work, a multiphase DNS method based on the VOF model is used to investigate two types of particle-particle interactions relevant in dispersed liquid-solid flows: the interaction between two solid particles under non-isothermal conditions, and the interaction between a solid particle and a deforming particle (e.g. a bubble). The computational method is based on solving a shared set of momentum and energy balance equations for the carrier phase and the particulate phases. Individual particles are tracked using a number of volume fraction advection equations. The method is shown to be able to correctly reproduce the particle dynamics in well-established test cases and is inherently capable of handling deformable particles co-existing with solid particles. It is also discussed how the detailed types of investigations performed in the current work can be used in the derivation of subgrid-scale models for larger industrial units.

Nomenclature

Latin letters

c_p	heat capacity
d	diameter
E	energy per unit mass
Eo	Eötvös number
$\boldsymbol{F}_\sigma$	force
$\boldsymbol{g}$	gravitational constant
k	thermal conductivity
N	number
P	pressure
Q	normalized heat source
Re	Reynolds number
T	temperature
t	time
V	volume
$\boldsymbol{u}$	velocity
U	characteristic velocity

Greek letters

β	thermal expansion coefficient
γ	volume fraction
λ	drag modification function
ρ	density
μ	viscosity

Subscripts and superscripts

f	fluid
i, j	index
p	particle
P	particles
ptf	particle-to-fluid
VF	volume fraction fields
0, ref	reference conditions

2. Modelling

2.1. Momentum transport

A shared set of balance equations is used for the continuous phase and the dispersed phases. These dispersed phases can be solid particles and/or fluid particles (i.e. droplets or bubbles). For a system of N_P solid particles, the volume fraction of the carrier fluid in a computational cell is denoted γ_f and the volume fraction of the *i*:th particle is designated $\gamma_{p,i,}$. To avoid inadvertent particle coalescence, particles that touch each other must be interpreted as separate phases and hence exist in different volume fraction fields. The subscript *j* in the variable $\gamma_{p,i,j}$ thus represents the volume fraction of the *i*:th particle present in the *j*:th volume fraction field. The total number of volume fraction fields employed is denoted N_{VF}, and the sum of all volume fractions in a computational cell is unity:

$$\gamma_f + \sum_{j=1}^{N_{VF}}\left(\sum_{i=1}^{N_P}\gamma_{p,i,j}\right) = 1 \tag{1}$$

The herein proposed method puts no restriction on N_P, and we drop the particle identity subscript and summation for typographical reasons from this point.

The velocity field is determined from the shared continuity and momentum equations, assuming that the flow is incompressible and that the velocity of the two phases is continuous across the interface:

$$\nabla \cdot \boldsymbol{u} = 0 \tag{2}$$

$$\rho\left(\frac{\partial \boldsymbol{u}}{\partial t} + \boldsymbol{u}\cdot\nabla\boldsymbol{u}\right) = -\nabla P + \nabla\cdot\{\mu[\nabla\boldsymbol{u} + (\nabla\boldsymbol{u})^T]\} + \left\{[1-\beta(T-T_0)]\gamma_f\rho_{f,0} + \gamma_p\rho_p\right\}\boldsymbol{g} + \boldsymbol{F}_\sigma \tag{3}$$

As may be seen from the gravitational term in equation (3), the Boussinesq model [26] is employed to describe the variation of the buoyancy force with temperature.

The shared density and viscosity in equation (3) are determined locally using:

$$\rho = \rho_f\left(\gamma_f + \gamma_p\rho_{ptf}\right) \tag{4}$$

$$\mu = \mu_f\left(\gamma_f + \gamma_p\mu_{ptf}\right) \tag{5}$$

where ρ_{ptf} and μ_{ptf} indicate the particle-to-fluid ratio of densities and viscosities, respectively.

The presence of the particles is monitored by solving N_{VF} continuity equations for the particulate phase:

$$\frac{\partial \gamma_{p,i,j}}{\partial t} + \nabla \cdot \left(\gamma_{p,i,j}\boldsymbol{u}\right) = 0 \tag{6}$$

The VOF methodology used here was originally proposed by Hirt and Nichols [7] for simulations of gas-liquid and liquid-liquid systems. Using VOF for handling also solid particles motion requires some additional considerations. First, the velocity boundary condition at the interface between the solid particle and the fluid should replicate that of no slip. Therefore, μ_{ptf} in equation (5) should approach infinity in the regions occupied by solid particles. In practice, a sufficiently high numerical value is acceptable [27]. Second, a unidirectional velocity field is enforced inside each solid particle by updating the shared velocity field at the end of each time step. Finally, the term $\boldsymbol{F}_\sigma$ in equation (3) represents a force designed to ensure that a solid particle retains its spherical shape [27-29].

It becomes important that each solid particle exists in a different volume fraction field if two or more particles come in close proximity of each other. Otherwise, particle coalescence could inadvertently occur. To guarantee that solid particles in close proximity of each other always exist in separate volume fraction fields, a control algorithm is implemented that moves the particles between different fields as required by the current state of the solution.

2.2. Energy transport

The temperature field is obtained by solving an energy balance equation:

$$\frac{\partial}{\partial t}\left(\gamma_p\rho_p E_p + \gamma_f\rho_f E_f\right) + \nabla \cdot \left[\boldsymbol{u}\left(\gamma_p\rho_p E_p + \gamma_f\rho_f E_f + P + \frac{\rho \boldsymbol{u}^2}{2}\right)\right] = \nabla \cdot (k\nabla T) \tag{7}$$

where

$$E_i = \int_{T_{ref}}^{T} c_{p,i}\, dT \tag{8}$$

and $i = f$ or p.

In the same way as with the pressure and velocity, the continuous and dispersed phases share a single temperature field. The local value of the thermal conductivity is determined using:

$$k = k_f\left(\gamma_f + \gamma_p k_{ptf}\right) \tag{9}$$

Equations (2), (3) and (7) are discretized on a co-located grid using the QUICK scheme for the convection terms and a second-order accurate central-differencing scheme for the diffusion terms. The pressure-velocity coupling algorithm is PISO, and PRESTO! is used as the pressure interpolation scheme. Equation (6) is discretized using the CICSAM scheme [30].

The temporal discretization of all balance equations is first-order implicit, with the exception of equation (6). The solution of the latter equation is advanced in time using explicit time stepping and a time step that is limited by the constraint that the global CFL number must remain below 0.25. A small CFL number, when used with explicit time stepping and a robust spatial discretization scheme with an upwind character, counteracts numerical diffusion that could otherwise lead to smearing of the interface profile [31]. It also assists in avoiding convergence problems, at the expense of having to take a larger number of time steps in the update of equation (6). To maintain computational efficiency, the update of equation (6) is therefore performed only once at the beginning of every fluid flow time step, so that the volume fraction fields are frozen during the iterative solution of the continuity, momentum and energy balance equations.

3. Results and Discussion

3.1. Isothermal particle-particle interaction

The choice of variables by which to non-dimensionalize the results is not entirely straightforward [21]. Here, we choose the approach of Yu et al. [32] and make the velocity dimensionless by a characteristic velocity $U = d_p^2(\rho_p - \rho_f)g/16\mu$ that is representative of the terminal velocity, whereas the position and time are scaled by the particle diameter and the characteristic time scale $t = d_p/U$ respectively. The drag force is made dimensionless by scaling with the Stokes drag, $F = 3\pi\mu d_p U$.

Since the proposed method is developed for investigations of systems of many particles, it is of great importance to verify that the method is indeed capable of predicting the interaction of a particle with another particle. In the presence of other particles, the drag force on a particle increases in comparison to the situation when the particle is isolated in an unbounded domain. The correct drag force can, under such circumstances, be obtained by multiplying the Stokes drag with a drag modification function, λ.

The drag modification function for a particle approaching another (identical) particle was measured experimentally by Adamczyk et al. [33]. In Fig. 1, the predicted drag modification from the method used in this paper is compared to their data. The governing parameters for this problem are the particle-particle separation and the particle-particle size ratio (the latter being unity in our comparison). The particle motion remains within the Stokes flow regime throughout the interaction. The agreement observed is good, and the slight disagreement at the smallest particle-particle distance can be explained by the decision not to dynamically refine the mesh in the region between the two particles.

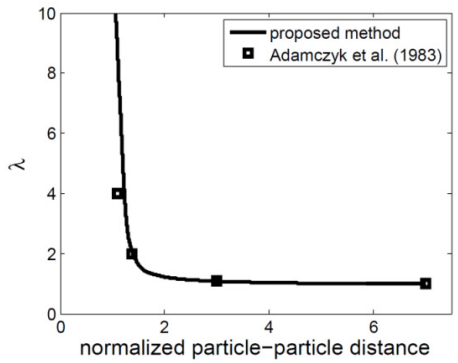

Fig. 1. Drag modification function (λ) plotted versus the particle-particle distance. The particle-particle distance is taken from the stationary particle surface to the moving particle center and is normalized by the particle radius (i.e. a distance equal to unity indicates that the particle surfaces are in contact).

3.2. Drafting, kissing and tumbling

The next isothermal test case illustrates the occurrence of "drafting, kissing and tumbling" [34] of two identical particles interacting outside the Stokes flow regime. The two particles are located inside a 2D enclosure that measures $8d_p$ x $20d_p$. They are initially placed on the centerline of a quiescent domain with a distance of $2d_p$ between their centers, but start to fall towards the bottom of the enclosure due to gravity (ρ_{ptf} = 1.5) when the solution is advanced in time (see Fig. 2). The current results are in very good agreement with those obtained by Hu et al. [35] for a similar Reynolds number.

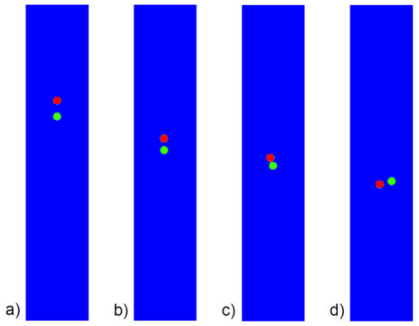

Fig. 2. Particle positions during the numerical drafting, kissing and tumbling experiment (Re ≈ 25): a) t = 0.25 s, b) t = 1.75 s, c) t = 2.25 s, d) t = 3 s. The drafting can be seen from (a) to (b), the kissing occurs in (c), and the tumbling can be seen in (d).

Fig. 3 illustrates the temporal evolution of the temperature field in and around the two particles in the drafting, kissing and tumbling experiment if they both have an internal heat source corresponding to Q = 1 [29]. The governing dimensionless parameters are (ρ_{ptf}, k_{ptf}) = (1.5, 5). It can be seen that, in the beginning, the particles have not yet attained high downward velocities and they are both seemingly unaffected by the heat release. After some time, the leading particle is accelerating and thus being cooled more efficiently at the front, where the boundary layer is thinner and the carrier phase cooler. The region in between the particles is beginning to heat up, preventing the particle behind the first one from experiencing a similar cooling at the front. Eventually, natural currents created by the heat release from both particles start to carry them upwards. In this sequence of events, the initial drafting is reversed and no kissing or tumbling occurs.

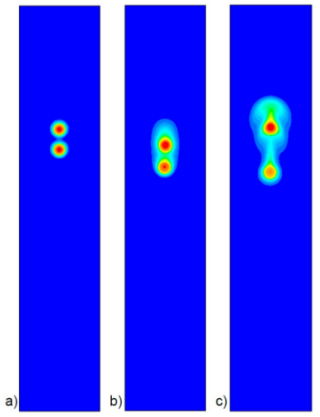

Fig. 3. Temperature fields for the numerical drafting, kissing and tumbling experiment with Q = 1: a) t = 0.25 s, b) t = 1.25 s, c) t = 2.5 s. For this magnitude of the internal heat sources, the buoyancy effect lifts both particles and increases the distance between them with time.

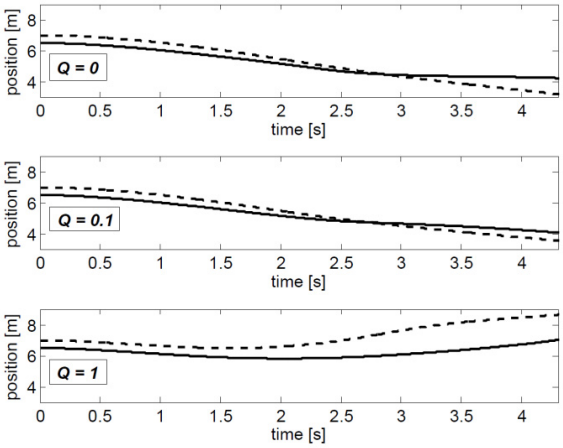

Fig. 4. Time history of the particle horizontal positions during the numerical drafting, kissing and tumbling experiment: a) isothermal conditions, b) internal heat source $Q = 0.1$, c) internal heat source $Q = 1$. In (a), the tumbling occurs at $t = 2.86$ s at a vertical position of 4.47 m, whereas in (b) it occurs at $t = 2.74$ s at vertical position of 4.73 m. In (c), no tumbling occurs at all. The dashed line illustrates the time history of the particle located initially in the upper position (UP), whereas the solid line illustrates the time history of the particle located initially in the lower position (LP).

In Fig. 4, the vertical positions of the two particles are shown as functions of time for three different magnitudes of the internal heat source, ranging from zero (i.e. isothermal) to one. When the internal heat sources are small but finite, the net result is an acceleration of the drafting sequence, which leads to earlier kissing and tumbling that both occur at a higher vertical position. This spatial displacement of the tumbling event can be seen in Fig. 4 and is approximately one particle diameter. In summary, it is shown here that the well-known drafting, kissing and tumbling behavior of two sedimenting particles can be significantly altered – even inhibited altogether – when heat transfer phenomena are present.

3.3. Particle-bubble interactions

Next, we investigate the interaction between a sedimenting solid particle and a rising bubble. More specifically, the aim is to investigate how the possible deformation of the bubble affects the particle-bubble interaction. Bubble deformation occurs naturally when the buoyancy force dominates the surface tension force, as signified by the Eötvös number ($\mathrm{Eo} = (\rho_1-\rho_2)gd_p^2/\sigma$) being larger than unity [36]. Because of the explicit presence of the bubble diameter in the Eötvös number, bubble deformation is often associated with large bubbles. Another cause of bubble deformation is however the lowering of the surface tension that takes place if there is a presence of highly surface-active components in the liquid phase. This presents us with a physical motivation to provoke a change in the shape of a bubble by decreasing the value of the surface tension in the numerical simulation.

In an interaction between a sedimenting particle and a rising bubble, the approach of the two entities is not necessarily aligned with the axis of symmetry (in which case a close interaction becomes unavoidable). The limiting case where particle-bubble close contact may still occur hydrodynamically in spite of an initial separation in the horizontal plane is denoted the grazing radius configuration. The difference in behavior between a spherical and a deformed bubble in this type of interaction is exemplified in Fig. 5. Here, the grazing radius configuration corresponds to an initial horizontal separation equal to approximately 65% of the bubble radius [37]. The interaction of two different types of bubbles (one spherical and one deforming) with a solid particle is studied. In both cases, the interaction with the bubble causes the particle to attain a horizontal velocity away from the bubble as the two entities are coming close to each other. Even so, the particle collides with the spherical bubble, as shown in Fig. 5a. However, there will be no collision when the bubble deforms (Fig. 5b). This indicates that the probability of formation of bubble–particle agglomerates is decreased for bubbles that can easily deform.

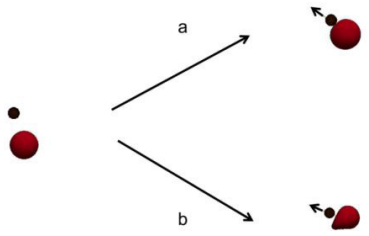

Fig. 5. Snapshots at different times of the interaction of a settling solid particle with a (a) spherical or a (b) deforming bubble.

The variation in the distance between the particle and the bubble surface is monitored throughout the interactions depicted in Fig. 5. Fig. 6 represents this normalized distance plotted versus the normalized time. This distance is taken from the particle center to the bubble surface, normalized by the particle diameter, so that a normalized distance of 0.5 corresponds to the two objects touching. Time is normalized using the particle response time. From Fig. 6 we see that the distance between the particle and the spherical bubble decreases continuously at all times, which results in collision. On the other hand, for the particle approaching the deforming bubble, this distance first decreases as the two objects are approaching. Then it starts to level up and eventually becomes almost constant. Such behavior implies that no collision takes place.

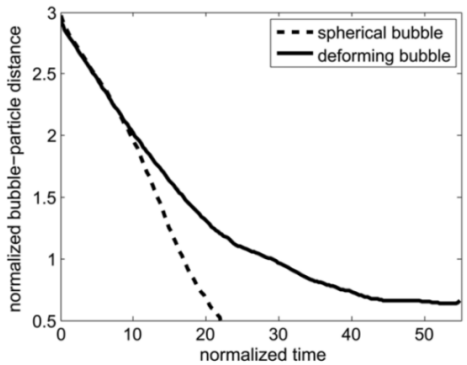

Fig. 6. The normalized distance between the particle and bubble surfaces is plotted versus the normalized time for the cases depicted in Fig. 5.

3.4. Simulations of industrial units

Detailed numerical investigations of hydrodynamic interactions between bubbles and particles are of great interest in many industrially important applications. One such example is in flotation, where the overall objective is to efficiently separate solid/liquid, liquid/solid/oil or oil/water mixtures by the formation of buoyant aggregates [38]. In a dissolved air flotation (DAF) unit, for example, air bubbles are injected into the continuous water phase, which contains solid particles to be removed from the water. The particles attach to the bubbles and form buoyant aggregates. These aggregates rise to the surface of the unit where they are removed. Since the aggregates consist of bubbles and particles with entrained water in between, they represent a complex composite of the three other phases. As a consequence, the aggregates have significantly different hydrodynamic properties and must be treated as a fourth “phase”. Additionally, the turbulence of the water-aggregate flow determines the bubble trajectories and the particle concentration field, and also affects the extent of aggregate formation and the aggregate properties. Hence, there is a feedback of information from the water-aggregate flow field to the fields that determine the local volume fraction of aggregates. A model of such an industrial system must therefore be able to handle all the links in this

chain in order to deduce any information about the performance of the equipment. A promising route to such simulations is via so-called hybrid schemes [39]. The method presented in the current work can be used for the derivation of hydrodynamic interaction forces between different configurations of bubbles and particles, as well as bubble-particle attachment probabilities as functions of locally varying parameters. Both these variables are needed in the development of accurate hybrid schemes for industrial units.

4. Conclusions

In the current work, a multiphase DNS (direct numerical simulation) method is used to investigate particle-particle interactions in dispersed liquid-solid flows. The two types of interactions include the interaction between two solid particles under non-isothermal conditions, and the interaction between a solid particle and a deforming particle (e.g. a bubble). It is shown that the presence of simultaneous particle-fluid heat transfer can have a significant effect on the drafting, kissing and tumbling sequence of two sedimenting solid particles. For small but finite internal particle heat sources, the drafting sequence is faster and the interaction is speeded up. However, the natural convection currents developing around the particles are also shown to inhibit the kissing and tumbling events altogether for larger internal heat sources. Furthermore, the isothermal interaction is studied between a solid particle and a bubble, and it is shown that the particle-bubble attachment process may be significantly altered under conditions of lowered surface tension (i.e. after addition of surfactants) due to an increased tendency for the bubble to deform.

Acknowledgements

The computations were partly performed on resources provided by the Swedish National Infrastructure for Computing (SNIC) at C3SE.

References

[1] L.K. Wang, E.M. Fahey, Z. Wu, Dissolved Air Flotation, in L.K. Wang, Y.-T. Hung, N.K. Shammas (Eds.), Handbook of Environmental Engineering, Humana Press, 2005.

[2] Y. Ben, G. Dorris, N. Pagé, S. Gendron, N. Gurnagul, C. Desrosiers, P. Maltais, First industrial flotation column in a paperboard recycling plant, Progr. Paper Recycling 18 (2009) 11-23.

[3] J. Rubio, H. Hoberg, The process of separation of fine mineral particles by flotation with hydrophobic polymeric carrier, Int. J. Miner. Process. 37 (1993) 109-122.

[4] P.T.L. Koh, M.P. Schwarz, CFD modelling of bubble-particle attachements in flotation cells, Miner. Eng. 19 (2006) 619-626.

[5] B. Bozzini, M.E. Ricotti, M. Boniardi, C. Mele, Evaluation of erosion-corrosion in multiphase flow via CFD and experimental analysis, Wear 255 (2003) 237-245.

[6] B. Guler, P. Wang, M. Delshad, G.A. Pope, K. Sepehrnoori, Three- and four-phase flow compositional simulations of CO2/NGL EOR, SPE Annual Technical Conference and Exhibition (2001) 71485-MS.

[7] C.W. Hirt, B.D. Nichols, Volume of fluid (VOF) method for the dynamics of free boundaries, J. Comput. Phys. 39 (1981) 201-225.

[8] G. Tryggvason, B. Bunner, A. Esmaeeli, D. Juric, N. Al-Rawahi, W. Tauber, J. Han, S. Nas, Y.-J. Jan, A front-tracking method for the computations of multiphase flow, J. Comput. Phys. 169 (2001) 708–759.

[9] C.S. Peskin, The immersed boundary method, Acta Numer. 11 (2002) 479–517.

[10] R. Mittal, G. Iaccarino, Immersed boundary methods, Ann. Rev. Fluid Mech. 37 (2005) 239-261.

[11] M. Uhlmann, An immersed boundary method with direct forcing for the simulation of particulate flows, J. Comput. Phys. 209 (2005) 448-476.

[12] D. Kim, H. Choi, Immersed boundary method for flow around an arbitrarily moving body, J. Comput. Phys. 212 (2006) 662-680.

[13] R. Mittal, H. Dong, M. Bozkurttas, F.M. Najjar, A. Vargas, A. von Loebbecke, A versatile sharp interface immersed boundary method for incompressible flows with complex boundaries, J. Comput. Phys. 227 (2008) 4825-4852.

[14] R. Glowinski, T.-W. Pan, T.I. Hesla, D.D. Joseph, A distributed Lagrange multiplier/fictitiuos domain method for particulate flows, Int. J.

Multiphase Flow 25 (1999) 755-794.

[15] R. Glowinski, T.-W. Pan, T.I. Hesla, D.D. Joseph, J. Periaux, A fictitious domain approach to the direct numerical simulation of incompressible viscous flow past moving rigid bodies - application to particulate flow, J. Comput. Phys. 169 (2001) 363-426.

[16] N. Sharma, N.A. Patankar, A fast computation technique for the direct simulation of rigid particulate flows, J. Comput. Phys. 205 (2005) 439-457.

[17] S.V. Apte, M. Martin, N.A. Patankar, A numerical method for fully resolved simulations (FRS) of rigid particle-flow interactions in complex flows, J. Comput. Phys. 228 (2009) 2712-2738.

[18] S.V. Apte, J. Finn, A variable-density fictitiuos-domain method for fully resolved simulation of high-density ratio fluid-particle systems, Proc. 7th Int. Conf. Multiphase Flow (ICMF-2010), Tampa, FL, USA, 2010.

[19] Z. Zhang, A. Prosperetti, A second-order method for three-dimensional particle simulation, J. Comput. Phys. 210 (2005) 292-324.

[20] Z. Yu, X. Shao, A. Wachs, A fictitious domain method for particulate flows with heat transfer, J. Comput. Phys. 217 (2006) 424-452.

[21] A. Wachs, Rising of 3D catalyst particles in a natural convection dominated flow by a parallel DNS method, Computers Chem. Eng. 35 (2011) 2169-2185.

[22] Z.-G. Feng, E.E. Michaelides, Heat transfer in particulate flows with Direct Numerical Simulation (DNS), Int. J. Heat Mass Transfer 52 (2009) 777-786.

[23] N.G. Deen, S.H.L. Kriebitzsch, M.A. van der Hoef, J.A.M. Kuipers, Direct numerical simulation of flow and heat transfer in dense fluid-particle systems, Chem. Eng. Sci. 81 (2012) 329-344.

[24] D. Lakehal, M. Meier, M. Fulgosi, Interface tracking towards the direct simulation of heat and mass transfer in multiphase flows, Int. J. Heat Fluid Flow 23 (2002) 242-257.

[25] H.A. Jakobsen, Chemical Reactor Modeling. Multiphase Reactive Flows, Springer-Verlag, Berlin Heidelberg, 2008.

[26] J. Boussinesq, Théorieanalytique de la chaleur, Gathier-Villars, Paris, 1903.

[27] H. Ström, S. Sasic, B. Andersson, A novel multiphase DNS approach for handling solid particles in a rarefied gas, Int. J. Multiphase Flow 37 (2011) 906-918.

[28] J.U. Brackbill, D.B. Kothe, C. Zemach, A continuum method for modeling surface tension, J. Comput. Phys. 100 (1992) 335–354.

[29] H. Ström, S. Sasic, A multiphase DNS approach for handling solid particles motion with heat transfer, Int. J. Multiphase Flow 53 (2013) 75-87.

[30] O. Ubbink, Numerical prediction of two fluid systems with sharp interfaces, PhD thesis, Imperial College of Science, Technology & Medicine, London, 1997.

[31] M. Darwish, F. Moukalled, Convective schemes for capturing interfaces of free-surface flows on unstructured grids, Num. Heat Transfer B 49 (2006) 19-42.

[32] Z. Yu, N. Phan-Thien, Y. Fan, R.I. Tanner, Viscoelastic mobility problem of a system of particles, J. Non-Newtonian Fluid Mech. 104 (2002) 87-124.

[33] Z. Adamczyk, M. Adamczyk, T.G.M. van de Ven, Resistance coefficient of a solid sphere approaching plane and curved boundaries, J. Colloid Interface Sci. 96 (1983) 204-213.

[34] A.F. Fortes, D.D Joseph, T.S. Lundgren, Nonlinear mechanics of fluidization of beds of spherical particles, J. Fluid Mech. 177 (1987) 467-483.

[35] H.H. Hu, D.D Joseph, M.J. Crochet, Direct simulation of fluid particle motions,. Theoret. Comput. Fluid Dynamics 3 (1992) 285-306.

[36] R. Clift, J.R. Grace, M.E. Weber, Bubbles, Drops, and Particles, Academic Press, New York, 1978.

[37] S. Sasic, E. K. Sibaki, H. Ström, Direct numerical simulation of a hydrodynamic interaction between settling particles and rising microbubbles, Eur. J. Mech. B-Fluid 43 (2014) 65-75.

[38] C. Oliveira, J. Rubio, A short overview of the formation of aerated flocs and their applications in solid/liquid separation by flotation, Miner. Eng. 39 (2012) 124-132.

[39] H. Ström, M. Bondelind, S. Sasic, A novel hybrid scheme for making feasible numerical investigations of industrial three-phase flows with aggregation, Ind. Eng. Chem. Res. 52 (2013) 10022-10027.